Supplementary information

Drought impacts on the electricity system, emissions, and air quality in the western US

Minghao Qiu [a,b,1], Nathan Ratledge [c], Inês M. L. Azevedo [d], Noah S. Diffenbaugh [a], Marshall Burke [a,e,f],

a Doerr School of Sustainability, Stanford University, Stanford, CA, USA

b Center for Innovation in Global Health, Stanford University, Stanford, CA, USA

c Emmett Interdisciplinary Program in Environment and Resources, Stanford University, Stanford, CA, USA

d Department of Energy Science and Engineering, Stanford University, Stanford, CA, USA

e Center on Food Security and the Environment, Stanford University, Stanford, CA, USA

f National Bureau of Economic Research, Cambridge, MA, USA

1 To whom correspondence should be addressed. E-mail: mhqiu@stanford.edu

Supplementary methods

Alternative specifications of regression models

To explore the robustness of our estimation results across alternative specifications of regression models, we conduct three sensitivity analyses to estimate the impacts of runoff on electricity generation from fossil fuel plants:

1) **Estimating regression models using alternative drought indices.** Our main analysis uses the 9-month average runoff anomalies computed from the NLDAS-2 VIC model. We also estimate the regression models using runoff anomalies averaged over different windows (3, 6, and 12 months), as well as runoff anomalies from the other NLDAS-2 models (Noah and Mosaic). We find largely consistent results when using alternative drought indices (see Figure S2).

2) **Estimating regression models using alternative model specifications.** Our main analysis includes monthly sales of electricity, generation of wind power and solar power, and the monthly average air temperature at the plant location as covariates. The main specification also includes linear year trend, month-of-year fixed effects, and unit-level fixed effects to control for the underlying trend and seasonality in fossil generation and runoff, as well as time-invariant unobserved factors at the unit level. Coefficients are estimated using the weighted ordinary least square approach, weighted by the unit-level monthly average generation (i.e. size of the plants). We further estimate regression models which do not include control variables ('No ctrl' in Figure S3), models which include natural gas as an additional control variable ('Ctrl+Gas price'), models which estimate the coefficients with ordinary least square ('Non-weighted'), models which include year fixed effects instead of linear year trend ('Year FE'), and models that specify a quadratic relationship between runoff anomalies and electricity generation ('Quadratic'). We find that the estimation results are largely consistent across alternative specifications of the regression models (see Figure S3 and Table S1).

3) **Estimating distributed lag regression models.** In our main analysis, we calculate the running average of runoff for the previous 9 months and use the anomalies to characterize the drought conditions. The model ignores potential dynamics within this 9-month window, e.g., electricity generation (from hydropower and fossil sources) can respond to runoff changes at the current month differently from changes in the previous months. To address this issue, we perform a sensitivity analysis estimating a distributed lag model to account for the potential dynamics.

Specifically, we estimate the following equation:

$$y_{igym} = \sum_{k\in\{CA,NW,SW\}}^{t=0,\ldots,9} \{\beta_{gkt} Q_{kym-t}\} + \gamma_g \boldsymbol{X_{igym}} + \eta_g y + \psi_{gm} + \theta_i + \epsilon_{igym} \quad (1)$$

where Q_{kym-t} denotes the runoff anomalies of region k and the month that was t months prior to the current month. β_{gkt} thus measures the effects of runoff anomalies in region k at the month that was t months before on fossil fuel generation in region g in the current month.

As shown in Figure S5, we find that while the individual estimates on the lagged effects are somewhat noisy, coefficients are larger close to zero lag and then go to zero as lag length increases. When we sum the lagged coefficients to get the total (cumulative) effect of a one unit change in runoff in one month (or, equivalently, the effect in the current month of increasing runoff by one unit in each of the nine previous months), we get a coefficient that is very similar to our main effect, which is the effect in the current month of increasing average runoff over the prior nine months by one unit. This suggests that our main moving-average estimate captures the overall dynamics of plant operation over time. Because coefficients estimated using the distributed lag models have larger standard errors and wider confidence intervals due to the larger number of estimated and summed coefficients, we retain our moving-average results as our main specification.

Sample selections

We conduct two sensitivity analyses to explore the impacts of sample selections on our estimates.

1) **Estimating the impacts on plants not included in our main sample.** Our main sample includes fossil fuel power plants in the EPA AMPD dataset. Our sample covers 90% of electricity generation from fossil fuel plants (including biomass). To understand the impacts of drought on the rest of the fossil plants not included in the sample, we compile the monthly generation data from the fossil fuel power plants in EIA-923 reports (*1*), but not in the AMPD sample. We refer to these plants as "non-AMPD" plants. Similar to our main analysis, we estimate the impacts of runoff changes on the electricity generation from those non-AMPD plants. The results are shown in Table S3.

We find a statistically significant effect of runoff changes on these non-AMPD plants in NW, but not in the other two regions. We do not find a statistically- significant effect of runoff on non-AMPD plants in CA, possibly because most of the non-AMPD plants in CA are combined heat and electricity plants that are less responsive to changes in hydropower on the grid. For NW, we

estimate that a unit increase of runoff anomalies leads to a 34% decline in fossil fuel generation, an effect size that is comparable to the estimates derived from our main sample. Using this estimate, we calculate that the drought-induced fossil fuel generation from these non-AMPD plants is 7.3% of our main estimates. As the emission data of these non-AMPD plants are not consistent with the emission data of the AMPD sample, we use our main sample and the main estimates for the consequent impact analysis.

2) **Estimating regression models using alternative sample restrictions.** In our main analysis, we only include an observation (i.e. unit-month) if the unit has at least four non-missing values during the month. Figure S4 shows the estimation results across different samples which include an observation if the unit has operated or reported for more than X days during the month (X=1,..,10). As the sample becomes more restricted (i.e. X gets larger), the estimated impacts are likely less influenced by outliers (due to potential missing values). However, a more restricted sample might also fail to capture signals from marginal power plants that only operate a few days a month. Considering this trade-off, our main analysis chooses X=4 as the restriction criterion, as magnitudes of the estimated coefficients remain largely stable after X$\geq$4.

Alternative definition of regions

In our main analysis, we divide the western US into three regions (CA, NW, SW) following the EIA classification. However, the NW region includes eight states, and some states differ significantly from others (in particular, the importance of hydropower in each state). In our main analysis, we address this issue by calculating the regional runoff anomalies as the weighted average of state-level runoff anomalies (weighted by the state-level hydropower capacity). To address this issue more directly, we adopt an alternative definition of the electricity regions. NW is split into two regions – *NW1* which includes four hydro-rich states (WA, OR, ID, MT), and *NW2* which includes the other four states (CO, NV, UT, WY). We then estimate the following regressions to quantify the impacts of drought from each of the four regions on electricity generation from fossil fuel units:

$$y_{igym} = \sum_{k\in\{CA,NW1,NW2,SW\}} \{\beta_{gk} Q_{kym}\} + \gamma_g \boldsymbol{X_{igym}} + \eta_g y + \psi_{gm} + \theta_i + \epsilon_{igym} \quad (2)$$

where y_{igym} denotes the log of electricity generation from unit i in electricity region g, year y, and month-of-year m. Q_{kym} denotes the runoff anomalies of region k ($k \in \{CA, NW1, NW2, SW\}$) in year y, and month-of-year m. For comparison purposes, we estimate separate equations for each of the three originally-defined regions g ($g \in \{CA, NW, SW\}$). The regression results are shown in

column (2) in Table S1. We find that the impacts of NW's runoff on fossil fuel generation mostly come from runoff changes in the region encompassing the hydro-rich states (NW1), while NW2's runoff has a very limited effect on fossil generation. This is consistent with our findings that the need to substitute for changes in hydropower is the leading mechanism that explains the increases in fossil fuel generation during drought (as shown in our mediation analysis).

Interregional import and export of electricity

To further understand the trans-boundary impacts of runoff on fossil power plants, we use the hourly electricity import and export data from EIA to estimate how drought influences the inter-regional exchange of electricity between the three regions in the western US (*2*). Hourly electricity production, demand, and exchange between electric electricity regions are available since July 2015. Using data from 2016 to 2021, we estimate the following regression:

$$Export_{ym}^{i->j} = \beta_{ij} Q_{jym} + \gamma_g \boldsymbol{X_{iym}} + \theta_i Export_{ym}^{i->other} + \eta_{iy} + \psi_{im} + \epsilon_{iym}$$

where $\text{Export}_{ym}^{i->j}$ denotes the net export from electricity region i to electricity region j on year y and month-of-year m, Q_{jym} denotes the runoff anomalies of region j on year y and month-of-year m. $\boldsymbol{X_{iym}}$ denotes a set of control variables, including the hydro generation, electricity demand, solar and wind generation of region i. $Export_{ym}^{i->other}$ denotes the export from region i to the other electricity region (other than j). η_{iy} and ψ_{im} denote year and month-of-year fixed effects. ϵ_{iym} is the normally-distributed error term. Here, the main coefficient of interest is β_{ij}, which quantifies the impacts of runoff changes in region j on the net export of electricity from region i to j, conditional on the export to the other region and generation of region i. As shown in Figure S6, we find that neighboring regions that are connected to the drought regions increase their net export to the drought regions to make up for shortfall in the drought region. This suggests that the trans-boundary effects of drought on fossil fuel generation are largely driven by the changes in the import/export of electricity due to drought-induced supply or demand shocks.

Causal mediation analysis

We use causal mediation analysis to identify mechanisms through which runoff changes can influence electricity generation from fossil fuel plants. We focus on the following four mechanisms through which runoff changes could influence electricity generation from fossil fuel plants: 1) through changes in hydropower output (mediator variable: monthly hydropower generation), 2)

through changes in electricity demand (mediator: monthly electricity demand), 3) through changes in wind or solar power production (mediator: monthly generation from solar or wind power), and 4) through changes in cooling efficiency of thermal power plants due to ambient temperature (mediator: average ambient temperature at the plant locations).

For the mediation analysis, we only focus on the drought impacts on fossil fuel plants in the same electricity region (i.e. the local effect), and only focus on CA and NW where the estimated local effects are substantial. We use the R package "mediation" to perform the mediation analysis (*3*). For each mediator M, we estimate the following *outcome model*:

$$y_{gym} = \beta_g^O Q_{gym} + \gamma_g M_{gym} + \lambda_g^O \boldsymbol{X_{gym}} + \eta_{gy} + \psi_{gm} + \epsilon_{gym} \tag{3}$$

and the following *mediator model*:

$$M_{gym} = \beta_g^M Q_{gym} + \lambda_g^M \boldsymbol{X_{gym}} + \eta_{gy} + \psi_{gm} + \epsilon_{gym} \tag{4}$$

where y_{gym} denotes the log of the total fossil generation in electricity region g, year y, and month-of-year m. M_{gym} denotes the mediator variable. Q_{gym} denotes the runoff anomalies in electricity region g, year y, and month-of-year m. $\boldsymbol{X_{gym}}$ denote the control variables including runoff anomalies of the other two electricity regions and the other mediators (except for M_{gym}). The *outcome model* (equation 3) estimates how runoff and the mediator jointly influence the fossil generation, conditioned on the other potential mechanisms and runoff in the neighboring regions. The *mediator model* (equation 4) estimates the relationship between the mediator and runoff, conditioned on the other potential mechanisms and runoff in the neighboring regions. The causal mediation effect (i.e. the causal effect of runoff on fossil fuel generation through mediator M) is then estimated by evaluating the changes in y_{gym} associated with changes in M due to changes in Q, while not through the direct impacts of Q on y.

Air quality impacts: determining smoke day

Due to influences of drought on wildfire and associated $PM_{2.5}$ concentration (*4*, *5*), we only use observational $PM_{2.5}$ concentration from monitors on days that are not influenced by wildfire smoke. Following the method from (*6*), we classify a day as a "smoke day" if the monitor location either has identified smoke plume overhead, or the monitor location intersects with modeled air particle trajectories from nearby fires when clouds may obscure plume identification. Smoke plume information is derived from the National Oceanic and Atmospheric Administration Hazard Mapping

System, which provides analyst-identified plume boundaries based on visible bands of satellite imagery (*7–9*). Our air quality analysis focuses on the period between 2006 and 2020 due to the availability of the wildfire smoke plume data.

Back-of-the-envelope analysis on drought impacts on wind and solar power

In our causal mediation analysis, we find that a small fraction of the drought-induced increases in fossil generation could be due to reductions in wind and solar generation. This is consistent with evidence of reduction in solar generation due to wildfire smoke (which often coincides with drought) and the reduction in wind power due to lower wind speed during drought episodes (*10–12*). To further test this hypothesis, we conduct a back-of-the-envelope analysis. We estimate two regression equations to quantify: 1) the impacts of runoff changes on the number of smoke days (as defined in the section above) and 2) the impacts of runoff changes on wind speed. Consistent with the hypothesis, we find statistically significant effects for both channels. Focusing on CA, we find that a one unit decline of runoff anomalies leads to 0.35 additional smoke days for a given month ($p<0.01$). We also find that a one unit decline of runoff anomalies leads to a decline in surface wind speed by 2.9% ($p<0.05$). While it is challenging to calculate the effects on solar and wind generation due to the difficulty in matching the locations of wind turbines and solar panels to changes in smoke and wind speed, our back-of-the-envelope result suggests that drought potentially reduces the availability of solar and wind generation in western US, and as a result, further increases generation from fossil fuel plants.

Using InMAP to model the air quality impacts

As an alternative strategy to model the air quality impacts, we use the Intervention Model for Air Pollution (InMAP) to calculate the impacts of drought-induced emissions of SO_2 and NO_x on $PM_{2.5}$ concentrations. InMAP is a reduced complexity model that can simulate $PM_{2.5}$ concentrations given emissions inputs (*13*) and has been widely used at national scale to identify the levels and disparities in $PM_{2.5}$ (*14*, *15*). In this work, we use the InMAP source receptor matrix (ISRM) archived from (*16*). The ISRM consists of matrices of dimensions 52411×52411 (as the US is divided into 52411 grid cells) for three heights of emission locations and seven precursor emission species. For a given height and emission species, ISRM calculates the changes in $PM_{2.5}$ for any grid cell in the US due to one unit increase in one of the precursor emissions in any of the 52411 grid cells. We multiply the ISRM of SO_2 and NO_x by the plant-level drought-induced emission

changes (emission heights are determined according to the stack heights of the plant) to calculate the changes in drought-induced surface $PM_{2.5}$.

Projecting future impacts in the *high RE scenario*

Expansions of renewable energy (RE) could shift marginal energy sources from fossil energy to non-fossil energy. In our *high RE scenario*, we assume that when non-fossil energy is on the margin, the drought-induced electricity gap will be provided by the non-fossil energy and thus results in zero drought-induced emission. Our projection also assumes that if a non-fossil source is on the margin for a given hour, the source will have enough excess generation to cover the electricity gap during drought, i.e. the drought region does not need to import electricity from the neighboring region (regardless of the marginal energy source in the neighboring region).

We use the following illustrative example to demonstrate the projections of drought-induced emissions under *high RE* scenario. Our empirical analysis quantifies that an extreme drought condition in CA (corresponding to the 5th-percentile lowest runoff value from 2001-2021) leads to an increase in electricity generation by 19% from gas-fired plants in CAISO (the CA region), and by 11% from gas-fired plants in Public Service Company of Colorado (PSCC, part of the NW region). Suppose fossil energy is at the margin in both CAISO and PSCC, we would estimate a 19% increase of generation from gas-fired plants in CAISO and an 11% increase from gas-fired plants in PSCC due to drought in CA, same as the empirical estimates. If fossil energy is on the margin in CAISO but not in PSCC, we would estimate a 19% increase of gas-fired unit emissions in CAISO, and 0% increase of gas-fired unit emissions in PSCC (i.e. CA still needs to import electricity from PSCC, but from the non-fossil source in PSCC). On the other hand, if fossil energy is only on the margin in PSCC (but not CAISO), then we would estimate an 0% emission increase for both regions (as the electricity gap in CA is solely provided by the non-fossil source in CAISO and there is no need to import electricity from PSCC).

References

1. U.S. Energy Information Administration, *Survey form EIA-923 with detailed electric power data*, 2023.

2. U.S. Energy Information Administration, *Hourly Electric Grid Monitor*, 2021.

3. D. Tingley, T. Yamamoto, K. Hirose, L. Keele, K. Imai, Mediation: R package for causal mediation analysis. (2014).

4. Y. Wang, Y. Xie, W. Dong, Y. Ming, J. Wang, L. Shen, Adverse effects of increasing drought on air quality via natural processes. *Atmospheric Chemistry and Physics* **17**, 12827–12843 (2017).

5. Y. Xie, M. Lin, B. Decharme, C. Delire, L. W. Horowitz, D. M. Lawrence, F. Li, R. Séférian, Tripling of western US particulate pollution from wildfires in a warming climate. *Proceedings of the National Academy of Sciences* **119**, e2111372119 (2022).

6. M. L. Childs, J. Li, J. Wen, S. Heft-Neal, A. Driscoll, S. Wang, C. F. Gould, M. Qiu, J. Burney, M. Burke, Daily Local-Level Estimates of Ambient Wildfire Smoke PM2. 5 for the Contiguous US. *Environmental Science & Technology* (2022).

7. W. Schroeder, M. Ruminski, I. Csiszar, L. Giglio, E. Prins, C. Schmidt, J. Morisette, Validation analyses of an operational fire monitoring product: The Hazard Mapping System. *International Journal of Remote Sensing* **29**, 6059–6066 (2008).

8. G. D. Rolph, R. R. Draxler, A. F. Stein, A. Taylor, M. G. Ruminski, S. Kondragunta, J. Zeng, H.-C. Huang, G. Manikin, J. T. McQueen, *et al.*, Description and verification of the NOAA smoke forecasting system: the 2007 fire season. *Weather and Forecasting* **24**, 361–378 (2009).

9. M. Ruminski, S. Kondragunta, R. Draxler, J. Zeng, presented at the Proceedings of the 15th International Emission Inventory Conference, vol. 15, p. 18.

10. T. W. Juliano, P. A. Jiménez, B. Kosović, T. Eidhammer, G. Thompson, L. K. Berg, J. Fast, A. Motley, A. Polidori, Smoke from 2020 United States wildfires responsible for substantial solar energy forecast errors. *Environmental Research Letters* **17**, 034010 (2022).

11. S. D. Gilletly, N. D. Jackson, A. Staid, presented at the 2021 IEEE 48th Photovoltaic Specialists Conference (PVSC), pp. 1619–1625.

12. L. Lledó, O. Bellprat, F. J. Doblas-Reyes, A. Soret, Investigating the effects of Pacific sea surface temperatures on the wind drought of 2015 over the United States. *Journal of Geophysical Research: Atmospheres* **123**, 4837–4849 (2018).

13. C. W. Tessum, J. D. Hill, J. D. Marshall, InMAP: A model for air pollution interventions. *PloS one* **12**, e0176131 (2017).

14. C. W. Tessum, J. S. Apte, A. L. Goodkind, N. Z. Muller, K. A. Mullins, D. A. Paolella, S. Polasky, N. P. Springer, S. K. Thakrar, J. D. Marshall, *et al.*, Inequity in consumption of goods and services adds to racial–ethnic disparities in air pollution exposure. *Proceedings of the National Academy of Sciences* **116**, 6001–6006 (2019).

15. C. W. Tessum, D. A. Paolella, S. E. Chambliss, J. S. Apte, J. D. Hill, J. D. Marshall, PM2.5 polluters disproportionately and systemically affect people of color in the United States. *Science Advances* **7**, eabf4491 (2021).

16. A. L. Goodkind, C. W. Tessum, J. S. Coggins, J. D. Hill, J. D. Marshall, Fine-scale damage estimates of particulate matter air pollution reveal opportunities for location-specific mitigation of emissions. *Proceedings of the National Academy of Sciences* **116**, 8775–8780 (2019).

17. S. L. Decker, Officials identify steam plant accident victim. *The Chronicle* (May 11, 2005).

18. P. Gagnon, W. Frazier, W. Cole, E. Hale, "Cambium Documentation: Version 2021", tech. rep. (National Renewable Energy Lab.(NREL), Golden, CO (United States), 2021).

19. U.S. Environmental Protection Agency, *Emissions and Generation Resource Integrated Database (eGRID) 2019*, 2019.

20. T. Deryugina, G. Heutel, N. H. Miller, D. Molitor, J. Reif, The mortality and medical costs of air pollution: Evidence from changes in wind direction. *American Economic Review* **109**, 4178–4219 (2019).

21. C. Liu, R. Chen, F. Sera, A. M. Vicedo-Cabrera, Y. Guo, S. Tong, M. S. Coelho, P. H. Saldiva, E. Lavigne, P. Matus, *et al.*, Ambient particulate air pollution and daily mortality in 652 cities. *New England Journal of Medicine* **381**, 705–715 (2019).

22. Q. Di, L. Dai, Y. Wang, A. Zanobetti, C. Choirat, J. D. Schwartz, F. Dominici, Association of short-term exposure to air pollution with mortality in older adults. *Jama* **318**, 2446–2456 (2017).

23. P. Orellano, J. Reynoso, N. Quaranta, A. Bardach, A. Ciapponi, Short-term exposure to particulate matter (PM10 and PM2. 5), nitrogen dioxide (NO2), and ozone (O3) and all-cause and cause-specific mortality: Systematic review and meta-analysis. *Environment international* **142**, 105876 (2020).

Supplementary tables

	(1)	(2)	(3)	(4)
	log(generation) from CA plants			
CA	-0.143***	-0.130***	-0.143***	-0.120**
	(0.022)	(0.025)	(0.026)	(0.045)
NW/NW1	-0.443***	-0.414***	-0.443**	-0.428**
	(0.124)	(0.122)	(0.126)	(0.160)
NW2		-0.047		
		(0.061)		
SW	-0.052	-0.033	-0.052	-0.104**
	(0.032)	(0.028)	(0.034)	(0.037)
	log(generation) from NW plants			
CA	-0.057***	-0.053**	-0.057***	-0.047*
	(0.014)	(0.016)	(0.013)	(0.021)
NW/NW1	-0.170**	-0.160**	-0.170**	-0.192***
	(0.051)	(0.049)	(0.054)	(0.054)
NW2		-0.014		
		(0.032)		
SW	-0.005	-0.001	-0.005	-0.025
	(0.011)	(0.011)	(0.011)	(0.022)
	log(generation) from SW plants			
CA	0.002	0.006	0.002	0.009
	(0.022)	(0.022)	(0.022)	(0.025)
NW/NW1	-0.199	-0.188	-0.199	-0.108
	(0.103)	(0.102)	(0.124)	(0.091)
NW2		-0.020		
		(0.035)		
SW	-0.016	-0.009	-0.016*	-0.0004
	(0.012)	(0.012)	(0.006)	(0.022)
3 regions	Y		Y	Y
4 regions		Y		
SE clustered at plant-level	Y	Y		Y
SE clustered at county-level			Y	
Year trend + month FE	Y	Y	Y	
Year FE + month FE				Y

Table S1: **Estimated impacts of runoff anomalies on fossil generation under alternative specifications of the regression models**. Column (1) shows our preferred estimates reported in the main text. Column (2) shows the results estimated using an alternative definition of regions in the western US. NW is split into two regions – *NW1* which includes four hydro-rich states (WA, OR, ID, MT), and *NW2* which includes the other four states (CO, NV, UT, WY). Column (3) shows the results with standard errors clustered at county level. Column (4) shows results estimated using year fixed effects. Standard errors are reported in the parenthesis. Significance: $*$ $p<0.05$, $**$ $p<0.01$, $***$ $p<0.001$

	log (generation)	
	Texas	**Florida**
Runoff anomalies	-0.012	-0.008
	(0.012)	(0.021)

Table S2: **Fossil generation in Texas and Florida are not associated with runoff changes in each region.** The table shows the estimated impacts of runoff anomalies on electricity generation from fossil fuel plants in Texas or Florida. The impacts are estimated using regressions similar to equation [1] in the main text (but only considering impacts of runoff on generation in the same region). Standard errors are clustered at the plant level.

	log(generation) from non-AMPD plants		
	CA	NW	SW
Runoff anomalies	-0.023	-0.346***	0.003
	(-0.016)	(0.094)	(0.102)

Table S3: **Estimated impacts of runoff anomalies on fossil fuel generation from non-AMPD plants**. We estimate the impacts of runoff anomalies on generation from fossil fuel plants that are not included in our main sample (i.e. not included in the EPA AMPD dataset). The plant-level generation data is derived from EIA-923 reports (*1*). For simplicity, we only estimate the effects of runoff anomalies on fossil plants that are from the same region. Significance: $*$ $p<0.05$, $**$ $p<0.01$, $***$ $p<0.001$

Table S4: **Climate models used in this study for future projections.** We use projections from 33 global climate models with available runoff output at the monthly level for the historical and three climate scenarios from the CMIP6 model ensembles. The spatial resolution of each model is shown in latitude × longitude (unit: degree). Resolutions are approximated for models with varying latitudes. Data is downloaded in October, 2022.

Model	**Ensemble variant**	**Resolution**
ACCESS-CM2	r1i1p1f1	1.25 x 1.88
ACCESS-ESM1-5	r1i1p1f1	1.25 x 1.88
BCC-CSM2-MR	r1i1p1f1	1.12 x 1.12
CanESM5	r1i1p1f1	2.79 x 2.81
CAS-ESM2-0	r1i1p1f1	1.42 x 1.41
CESM2-WACCM	r1i1p1f1	0.94 x 1.25
CMCC-CM2-SR5	r1i1p1f1	0.94 x 1.25
CMCC-ESM2	r1i1p1f1	0.94 x 1.25
CNRM-CM6-1	r1i1p1f2	1.4 x 1.41
CNRM-CM6-1-HR	r1i1p1f2	0.5 x 0.5
CNRM-ESM2-1	r1i1p1f2	1.4 x 1.41
EC-Earth3	r1i1p1f1	0.7 x 0.7
EC-Earth3-Veg	r1i1p1f1	0.7 x 0.7
EC-Earth3-Veg-LR	r1i1p1f1	1.12 x 1.12
FGOALS-f3-L	r1i1p1f1	0.94 x 1.25
FGOALS-g3	r1i1p1f1	2.03 x 2
GFDL-ESM4	r1i1p1f1	1 x 1.25
GISS-E2-1-G	r1i1p1f2	2 x 2.5
GISS-E2-1-H	r1i1p1f2	2 x 2.5
INM-CM4-8	r1i1p1f1	1.5 x 2
INM-CM5-0	r1i1p1f1	1.5 x 2
IPSL-CM6A-LR	r1i1p1f1	1.27 x 2.5
KACE-1-0-G	r1i1p1f1	1.25 x 1.88
MCM-UA-1-0	r1i1p1f2	2.24 x 3.75
MIROC-ES2L	r1i1p1f2	2.79 x 2.81
MIROC6	r1i1p1f1	1.4 x 1.41
MPI-ESM1-2-HR	r1i1p1f1	0.94 x 0.94
MPI-ESM1-2-LR	r1i1p1f1	1.87 x 1.88
MRI-ESM2-0	r1i1p1f1	1.12 x 1.12
NorESM2-LM	r1i1p1f1	1.89 x 2.5
NorESM2-MM	r1i1p1f1	0.94 x 1.25
TaiESM1	r1i1p1f1	0.94 x 1.25
UKESM1-0-LL	r1i1p1f2	1.25 x 1.88

Supplementary figures

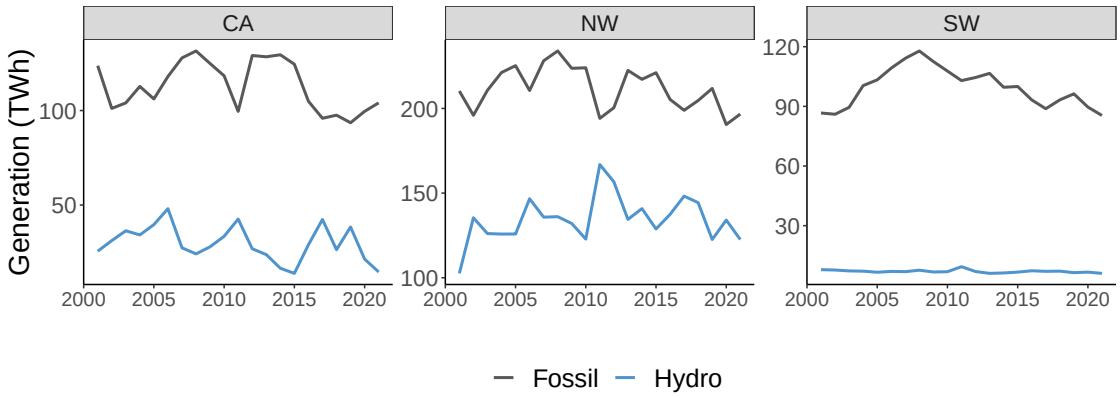

Figure S1: **Time series of hydropower and fossil fuel generation in the western US.** Figure shows the annual total generation from hydropower (blue) and fossil fuel sources (black) for each of the three regions in the western US.

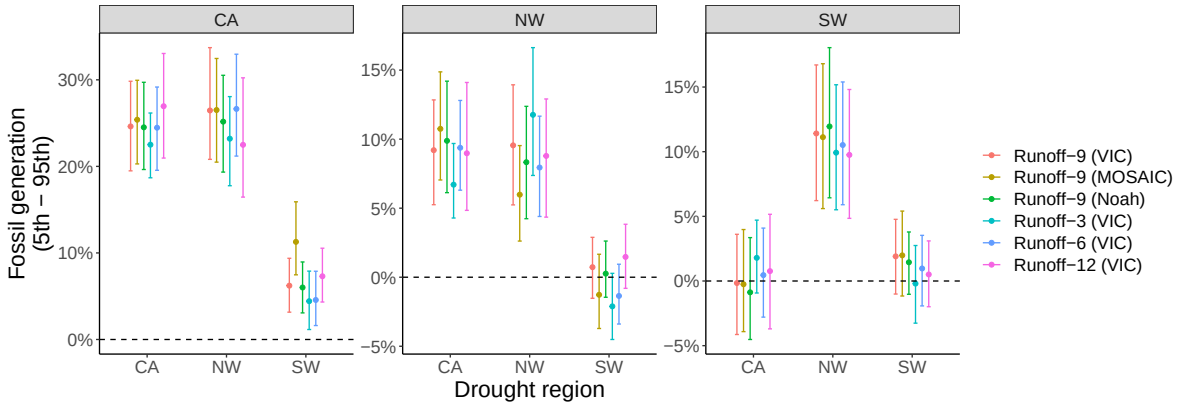

Figure S2: **Estimation results using runoff anomalies calculated using alternative methods.** Figure shows the estimated changes in fossil generation in one electricity region (corresponding to each panel) due to the 5th to 95th percentile change of runoff in each of the three regions (x-axis of each panel). The error bars show the 95% confidence intervals of the estimated generation changes. Standard errors are clustered at the plant level. Estimation results using runoff anomalies calculated with different methods are shown in different colors. Runoff anomalies are calculated using different averaging windows (3, 6, 9, 12 months) and derived from three different models of NLDAS-2 (VIC, MOSAIC, Noah). Our main analysis uses 9-month runoff anomalies from the VIC model (Red color, *Runoff-9 (VIC)*).

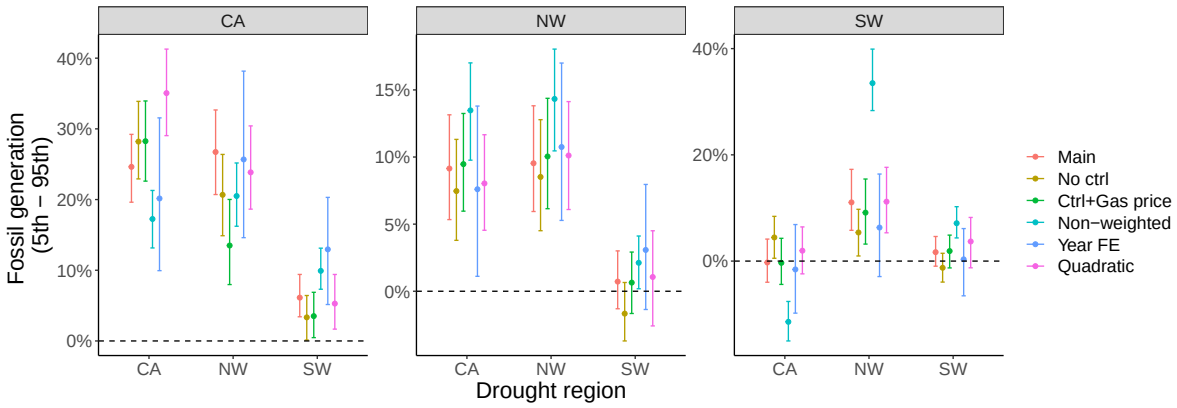

Figure S3: **Estimation results using alternative specifications of the regression model.** Figure shows the estimated changes in fossil generation in one electricity region (corresponding to each panel) due to the 5th to 95th percentile change of runoff in each of the three regions (x-axis of each panel). The error bars show the 95% confidence intervals of the estimated generation changes. Standard errors are clustered at the plant level. Estimation results using alternative specifications of the regression model are shown in different colors. Descriptions of the alternative specifications are discussed in SI.

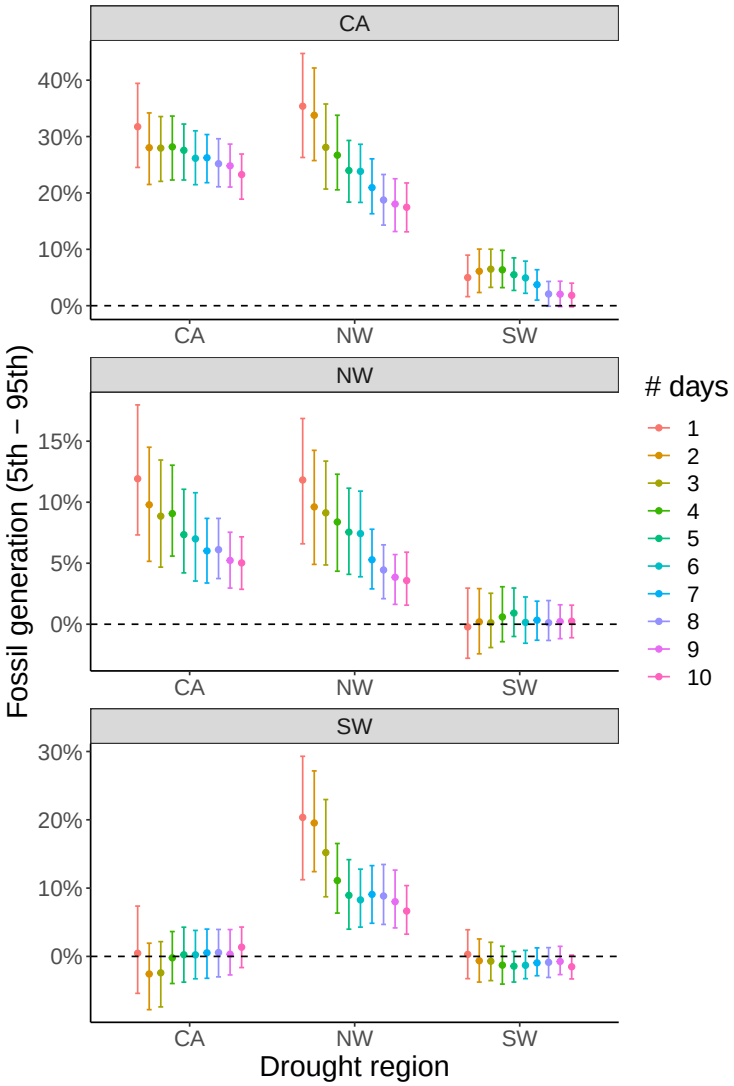

Figure S4: **Estimation results across different sample restrictions.** Figure shows the estimated changes in fossil generation in one electricity region (corresponding to each panel) due to the 5th to 95th percentile change of runoff in each of the three regions (x-axis of each panel). The error bars show the 95% confidence intervals of the estimated generation changes. Standard errors are clustered at the plant level. Figure shows the estimation results across different sample restriction thresholds (shown in different colors). For each threshold, the estimation is performed on a sample that includes an observation only if the unit has operated or reported for at least X days during the month (X=1,..,10). Our main analysis only includes an observation if the unit has operated or reported for at least four days during the month (i.e. X=4, shown in the green lines).

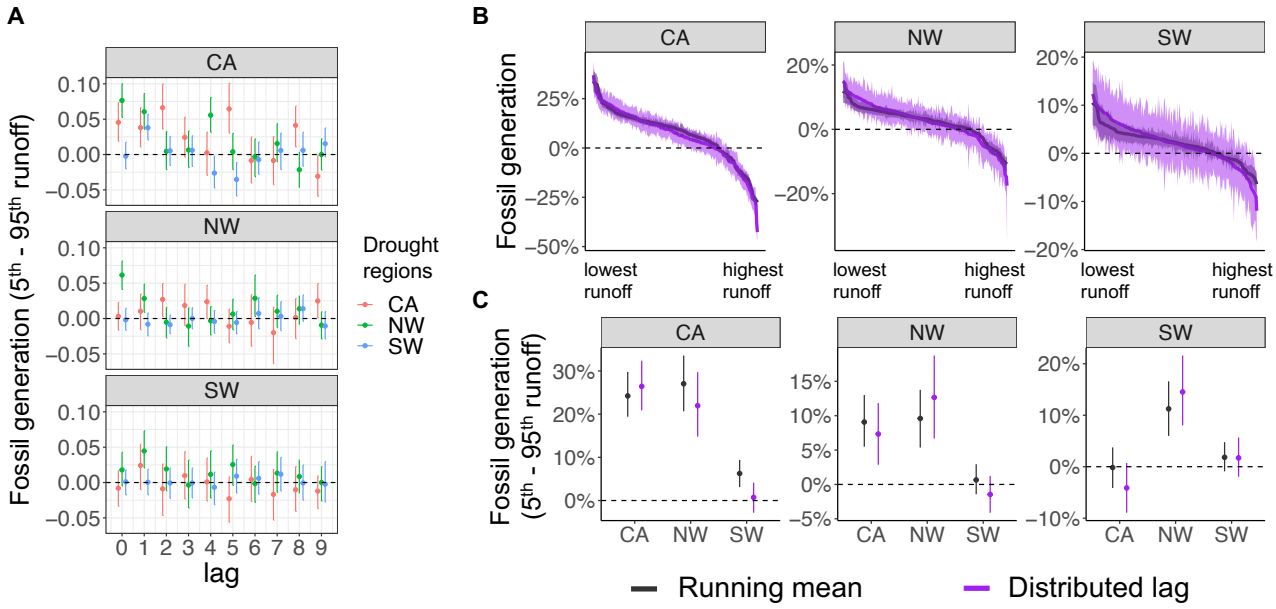

Figure S5: **Estimation results of the distributed lag model.** Panel A shows the effects of individual lags of runoff on fossil fuel generation. X-axis shows the lags (e.g. lag=0 denotes the effects of contemporary runoff anomaly on fossil generation in the current month). Y-axis shows the changes in fossil generation in one electricity region (each panel) due to the 5th to 95th percentile change of runoff anomalies (i.e. changes under dry conditions relative to wet conditions) in each of the three regions (shown by the line colors). In panels B and C, black lines show the results estimated using our main model (9-month average of runoff anomalies). Purple lines show the results estimated using the distributed lag model. Black lines show the same results in Figure 2 in the main text. Panel B: relative changes in monthly fossil generation in each region due to runoff changes in our study period. X-axis is sorted by the changes in fossil fuel generation, from months with the lowest runoff on the left to the months with the highest runoff on the right. Panel C: changes in fossil generation in one electricity region (each panel) due to the 5th to 95th percentile change of runoff anomalies (i.e. changes under dry conditions relative to wet conditions) in each of the three regions (x-axis of each panel). The error bars in panels A and C, and shades in panel B show the 95% confidence intervals of the estimated generation changes.

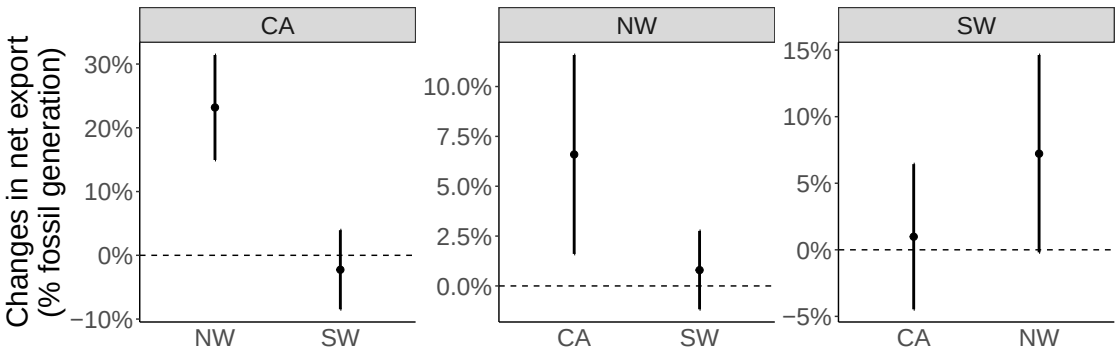

Figure S6: **Drought increases the net export of electricity from the neighboring regions to the drought region.** Figure shows the estimated changes in the net export of electricity from one electricity region (the source region, corresponding to each panel) to another electricity region (the drought region, x-axis of each panel) due to the 5th to 95th percentile change of runoff in the drought region.

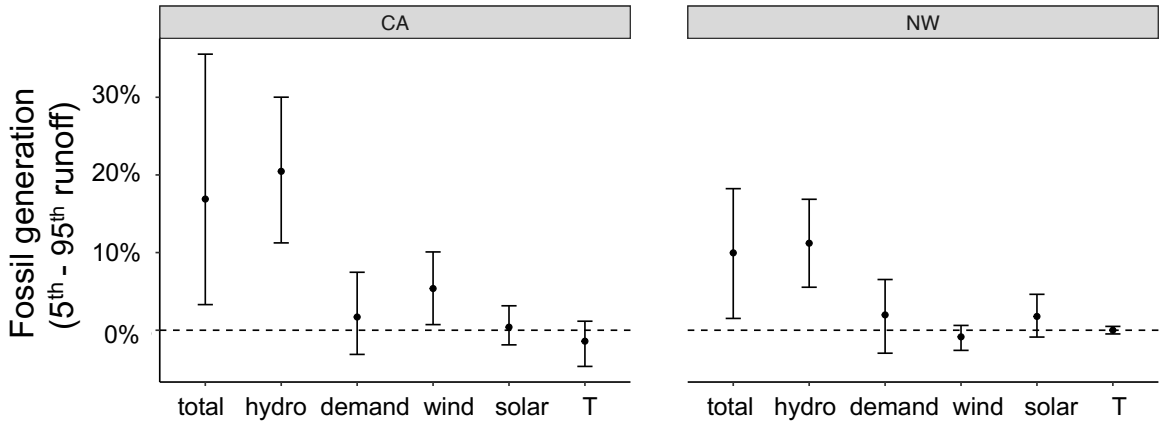

Figure S7: **The need to substitute for changes in hydropower is the leading mechanism that explains the runoff – fossil generation relationship.** Figure shows changes in fossil fuel generation due to the 5th to 95th percentile change of runoff anomalies (i.e. changes under dry conditions relative to wet conditions), through different mechanisms. We only focus on the drought impacts on fossil fuel plants in the same electricity region (i.e. the local effect), and only focus on California and Northwest where the estimated local effects are substantial. Figure shows the effects through all possible mechanisms ('total'), effects through changes in hydropower ('hydro'), effects through changes in electricity demand ('demand'), effects through changes in wind generation ('wind'), effects through changes in solar generation ('solar'), and effects through changes in the local temperature at the plant locations ('T', possibly by influencing the cooling efficiency).

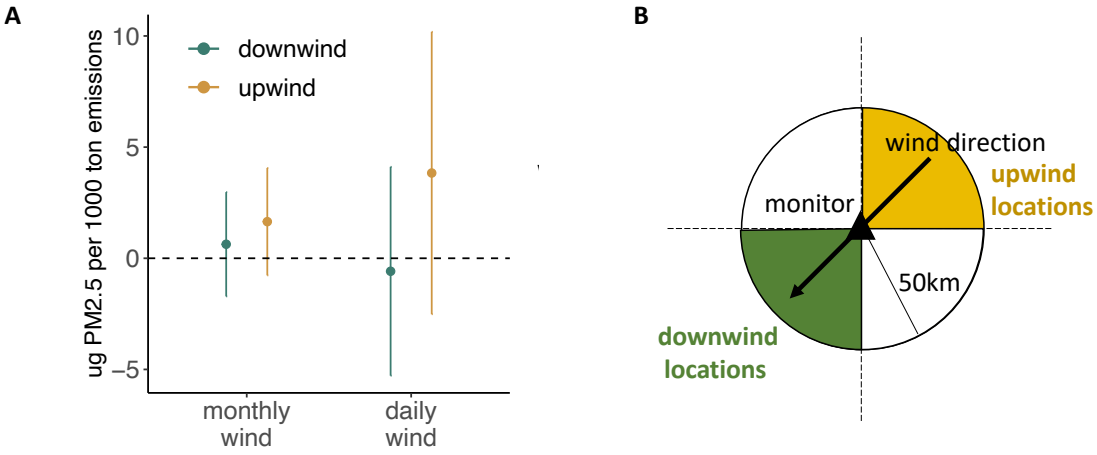

Figure S8: **Increases in surface $PM_{2.5}$ are more likely to be associated with drought-induced emissions emitted from upwind plants.** Panel A shows the $PM_{2.5}$ impacts of drought-induced emissions from fossil fuel plants within 50km radius of the monitor at upwind or downwind locations of the monitor. As shown in panel B, a plant is determined to be at the upwind location, if the plant is located in the "upwind quadrant" which is a 90 degree cone centering around the wind direction. The wind direction is calculated using the zonal and meridional wind components within 50km of the monitor (wind direction derived from the ERA5 land reanalysis data). Panel A shows the results estimated using monthly-average wind direction, as well as daily wind direction (paired with drought-induced emissions calculated at the daily level).

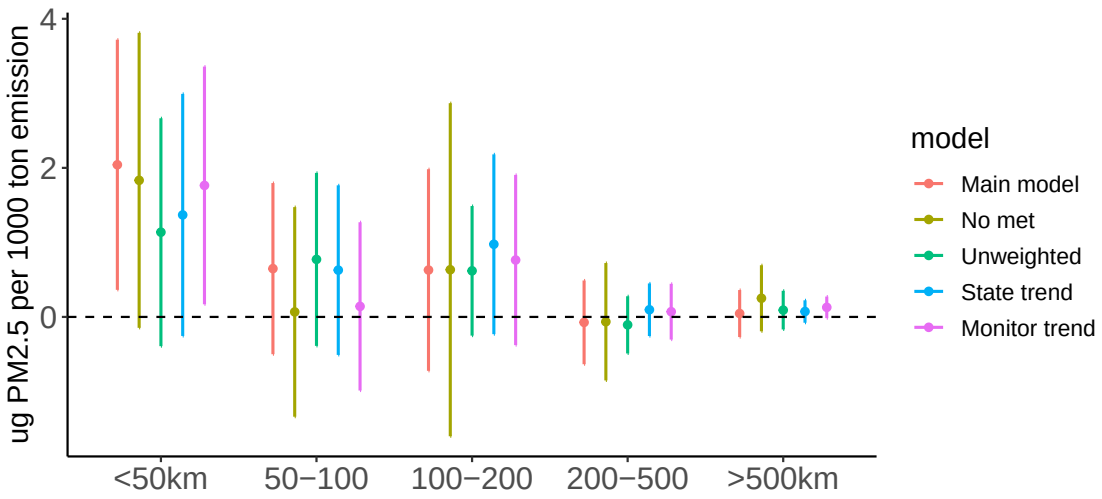

Figure S9: **Estimated impacts of drought-induced emission on surface $PM_{2.5}$ are largely consistent across alternative model specifications.** In our main specification, we include the splines of surface temperature, precipitation, dewpoint temperature, boundary layer height, air pressure, 10m wind direction (U and V components) and wind speed for meteorological controls, year and month-of-year fixed effects. The figure shows coefficients estimated under alternative specifications of regression models – coefficients estimated with no meteorology controls ('No met'), coefficients estimated using ordinary least square ('Unweighted'), and coefficients estimated using state-level year trend ('State trend') or monitor-level year trend ('Monitor trend') instead of the year fixed effects.

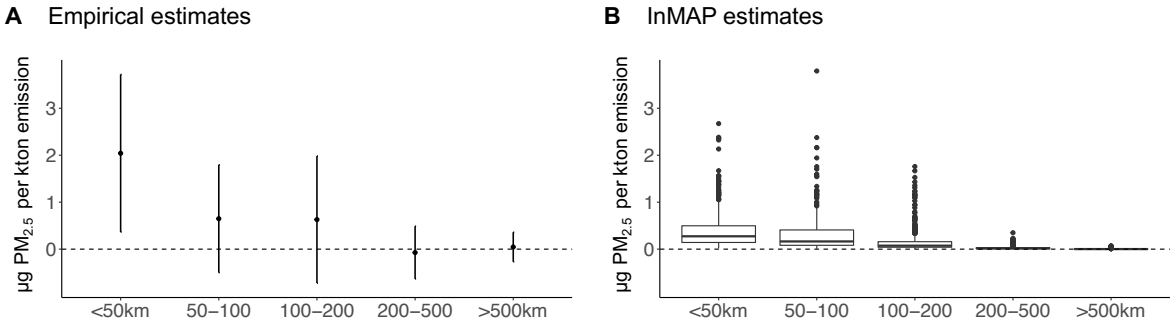

Figure S10: **Empirical and InMAP estimates of $PM_{2.5}$ impacts associated with drought-induced emissions.** Panel A shows the empirical estimates of drought-induced emissions of different distance bins on surface $PM_{2.5}$ (same as Figure 3C in the main text). Panel B shows the InMAP estimates of drought-induced emissions on surface $PM_{2.5}$. To derive the InMAP estimates, we first use InMAP to simulate $PM_{2.5}$ changes in the western US associated with one ton of SO_2 and NO_x emissions emitted from all power plants in our sample. Then for each air quality monitor, we calculate the ratio between the simulated $PM_{2.5}$ and the emissions from plants of a certain distance bin. The box plot in Panel B shows the range of the $PM_{2.5}$ – emissions sensitivities across different monitor locations.

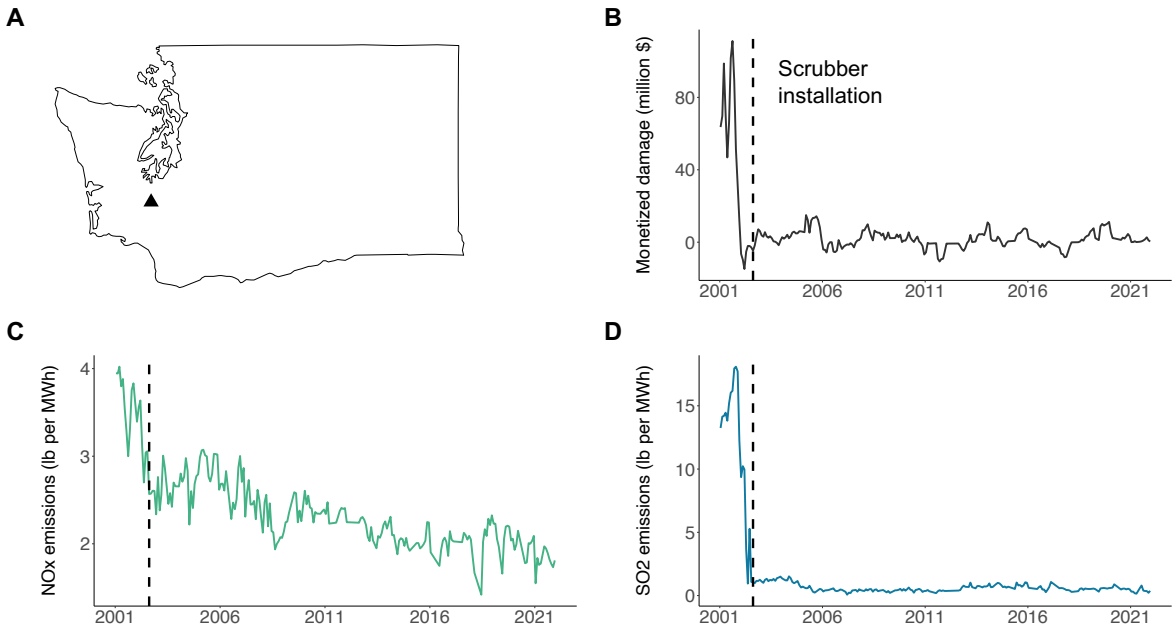

Figure S11: **Dramatic declines in the drought-induced $PM_{2.5}$ damage are driven by decline in emissions factors after scrubber installations.** Results are shown for a power plant in Washington State (panel A), which includes two units using coal as their main fuel type. Panel B shows the $PM_{2.5}$ damage due to drought-induced emissions from this plant. We find that the predicted drought-induced damages decline after the installation of scrubbers in August 2002 (*17*), driven by declines in NO_x (panel C) and SO_2 emission factors (panel D) .

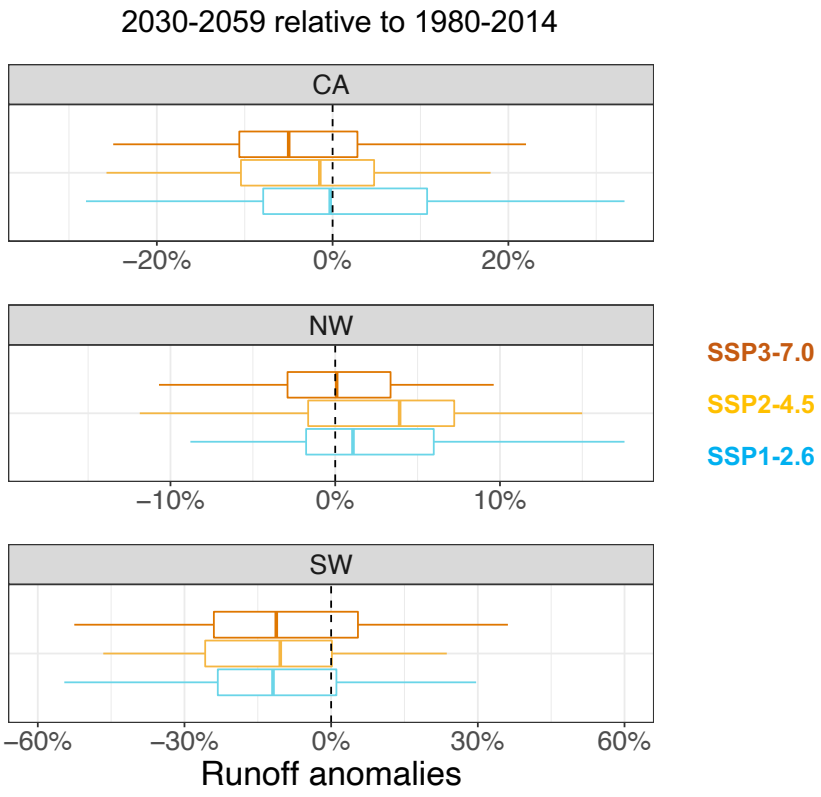

Figure S12: **Projected runoff anomalies under future climate.** The box plots show the range of projected runoff anomalies from 33 global climate models in CMIP6, under SSP1-2.6, SSP2-4.5, and SSP3-7.0 scenarios. Runoff anomalies are calculated relative to the 1980-2014 values from the historical simulations and then averaged over 2030-2059.

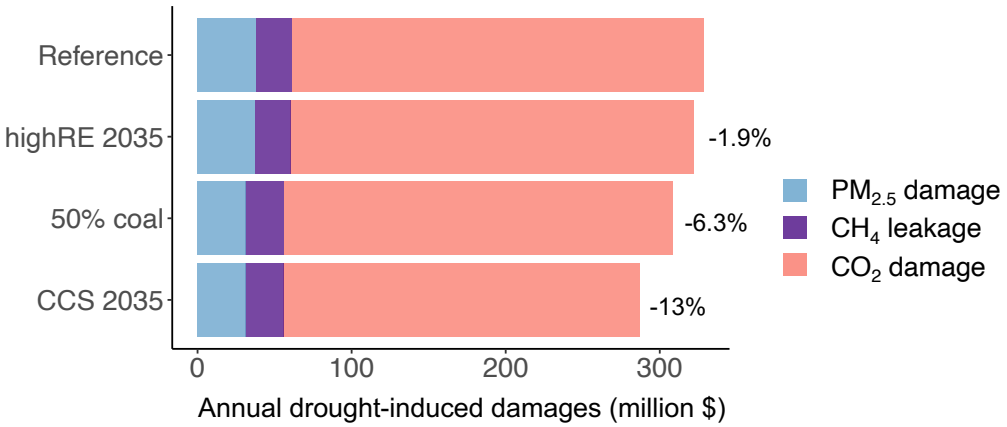

Figure S13: **Modest reductions in drought-induced damages under projected electricity sector scenarios (projection year 2035).** Figure shows the mean values of drought-induced damages projected by the 33 models under SSP3-7.0. The relative difference in damages under the three electricity sector scenarios (compared to the reference scenario) is shown in the figure.

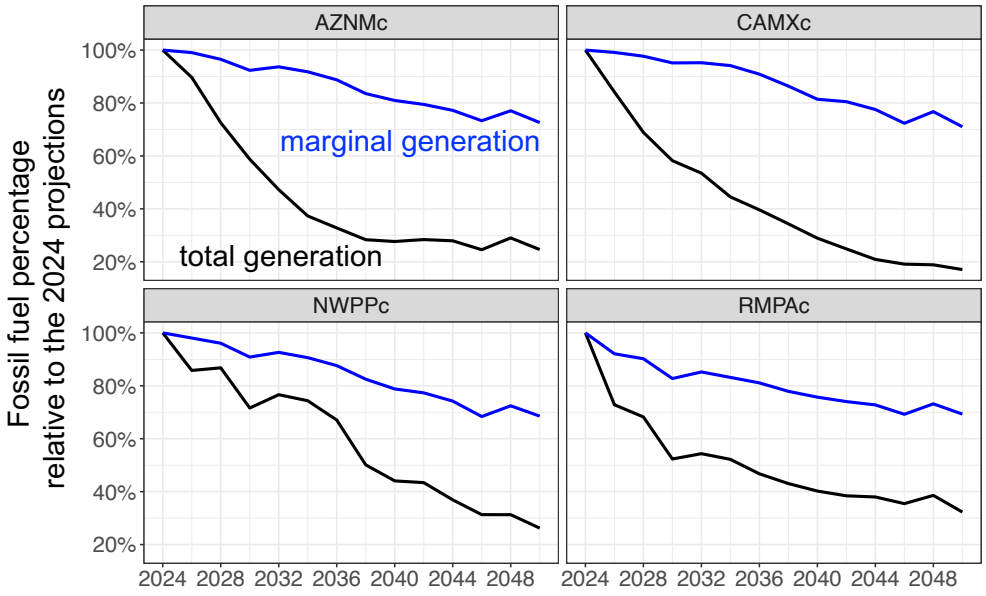

Figure S14: **Projected percentages of fossil fuel generation in the electricity grid of the western US.** We calculate the ratio of fossil fuel generation relative to the total electricity generation (black), and the percentage of time that fossil fuel generators are the marginal generators of the electric grid (blue). Results are derived from the hourly simulation under the "Low RE cost scenarios" of the Cambium data sets from 2024 to 2050 (*18*). Figures show the changes in fossil fuel generation percentage relative to the 2024 projections (i.e., 2024 results normalized to 1), for the four egrid subregions of western US (*19*).

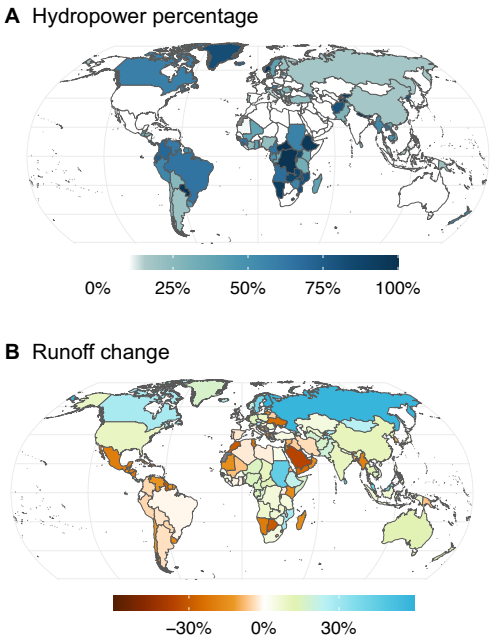

C

Country	Hydropower percentage	Runoff change
Namibia	93%	-21%
Bhutan	100%	-20%
Honduras	30%	-20%
Burma	53%	-19%
Guatemala	38%	-17%
Uruguay	47%	-17%
Kenya	33%	-16%
Madagascar	40%	-16%
French Guiana	48%	-16%
Venezuela	62%	-13%
Suriname	52%	-13%
Chile	25%	-12%
El Salvador	27%	-8%
Bosnia and Herzegovina	31%	-8%
Mali	39%	-7%
Papua New Guinea	21%	-7%
Portugal	20%	-7%
Fiji	50%	-7%
The former Yugoslav Republic of Macedonia	26%	-5%

Figure S15: **Many hydro-dependent countries face increasing drought risks due to climate change.** Panel A shows the percentage of electricity provided by hydropower in each country (averaged over 2015-2021). Panel B shows the projected changes (median changes across 33 models) in runoff under SSP3-7.0 between 2030 to 2059 (relative to 1980 to 2014). We identify 19 countries (table C) that could be vulnerable to drought-induced shocks to the electricity system (which has >20% generation coming from hydropower and is projected to have a >5% decline in runoff under future climate).

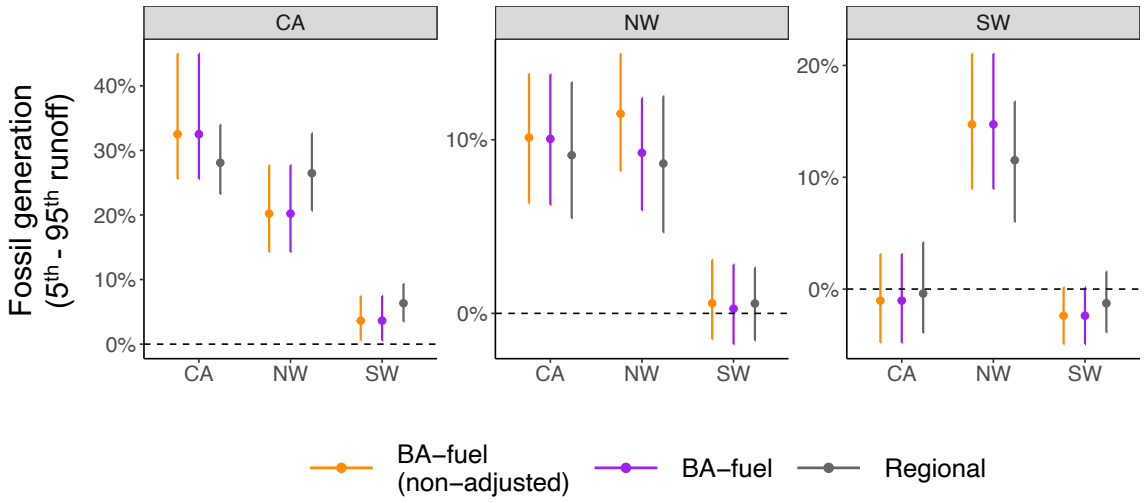

Figure S16: **Estimated impacts on fossil fuel generation are consistent across the estimations at the regional level and the BA-fuel level.** Changes in electricity generation estimated using the coefficients derived from regressions at the BA-fuel level are shown in orange. Changes in electricity generation estimated with adjusted coefficients (for 11 out of 681 units, we use the pooled regression coefficients at the regional level instead of the highly uncertain coefficients estimated at the BA-fuel level) are shown in purple. Changes in electricity generation estimated using the coefficients derived from the pooled regressions are shown in gray.

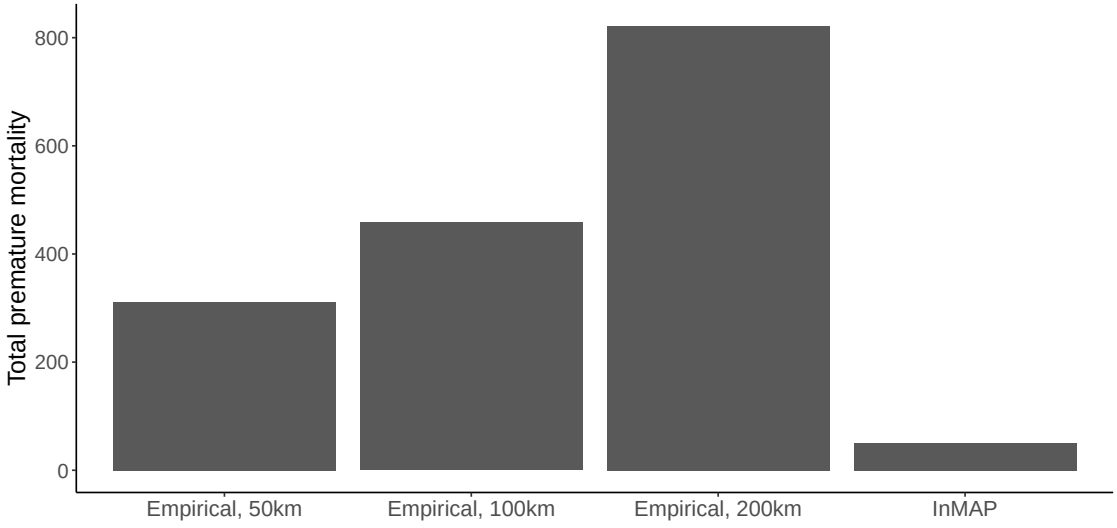

Figure S17: **Total premature mortalities due to drought-induced fossil generation during 2001 to 2021 under different methods to estimate drought-induced $PM_{2.5}$.** The figure shows three empirical estimates and one estimate based on InMAP simulations of the drought-induced $PM_{2.5}$ mortalities. Mortalities are estimated using the same CRF function from Deryugina et al. For the empirical estimates of drought-induced $PM_{2.5}$, we consider impacts of drought-induced emissions within the radius of 50km, 100km, or 200km, and use the corresponding regression coefficients. Our main analysis calculates the drought-induced $PM_{2.5}$ using the empirical approach that accounts for drought-induced emissions within a 100km radius.

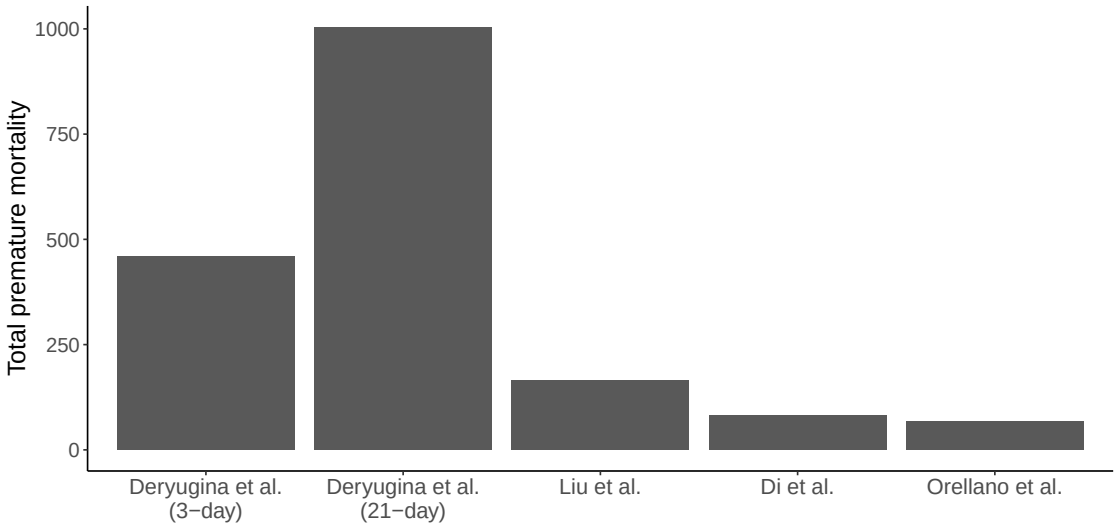

Figure S18: **Total premature mortalities due to drought-induced fossil generation during 2001 to 2021 under different CRFs (*20−23*).** *Deryugina et al., (3-day)* uses the main estimate from Deryugina et al. which calculates the total cumulative mortalities in the 3-day window following a day of exposure. *Deryugina et al., (21-day)* uses the alternative estimate reported in Deryugina et al. which calculates the total cumulative mortalities in the 21-day window following a day of exposure. Mortalities are calculated using the estimated drought-induced $PM_{2.5}$ from the empirical approach that accounts for drought-induced emissions within a 100km radius.